Plasma Phys. Control. Fusion **51** (2009) 075012 (15pp) doi:10.1088/0741-3335/51/7/075012

Hall-magnetohydrodynamic ion acceleration model in a z-pinch discharge during an $m = 0$ instability

J J Martinell, R M Fajardo and J J E Herrera

Instituto de Ciencias Nucleares, Universidad Nacional Autónoma de México A. Postal 70-543, México D.F., Mexico

Received 6 February 2009, in final form 8 April 2009
Published 28 May 2009
Online at stacks.iop.org/PPCF/51/075012

Abstract

The ion acceleration by a sausage instability in a z-pinch is modeled using Hall-magnetohydrodynamic theory taking into account the axial plasma velocity that necessarily develops during the instability. The instability grows, shrinking the neck, until it is stopped by increased pressure. The axial velocity influences ion acceleration through the radial electric field. An axial left–right asymmetry arises due to the contribution of the Hall term. The total electric field reverses its axial direction always on the anode side of the neck. The resulting electromagnetic fields are used to compute ion trajectories. Two classes of particle motion arise: singular ions that cross the cylinder axis and off-axis regular ions, and for both the acceleration by the electric fields is always toward the cathode. The energy gain of singular-orbit ions is larger, reaching values of up to 60. Most off-axis ions drift toward the axis due to the axial electric field, where they experience large energy gains. When the column radius is of the order of the Larmor radius the orbits are complex but the energy gain is still large.

1. Introduction

Certain magnetic confinement devices used in controlled nuclear fusion research share common properties with some particle accelerators. Both store charged particles in varying electric and magnetic fields, and the essential difference is that in fusion research the purpose is to confine a quasineutral, fully ionized, high temperature plasma, in the presence of higher currents. Thus, it is not surprising that high neutron yields, up to 20×10^6 per shot, produced by accelerated ions, were obtained since the early days of fusion research, back in 1958, in pulsed power devices [1–3]. Although these neutrons were first thought to be of thermonuclear origin, they were soon recognized to come from a beam-target effect [4], and it became clear that the instabilities responsible for the ion acceleration needed to be suppressed for reactor purposes. Furthermore, it was found that a high yield of pulsed neutrons was not enough to achieve energy breakeven. Longer confinement times, enough to compensate for energy

losses through radiation and other sources, were also needed. Simultaneous advancements in accelerator technology, where higher and well resolved energies were being achieved, rendered further studies of these phenomena unnecessary, and interest in them faded, although it did not disappear entirely. The dense plasma focus is one of such pulsed power devices, which to date provides the best cost per neutron yield ratio, and it is an interesting subject of study because of its relation to astrophysical phenomena, such as solar flares, as well as for certain applications such as ion implantation [5–7]. It has been shown that the angular distributions of neutron plasma foci emissions have both isotropic and anisotropic components, which means there is more than one mechanism which produces the fusion reactions in such devices [8, 9]. The anisotropic component is believed to be the consequence of a beam-target effect, and therefore understanding the acceleration mechanisms and characterizing the energy spectrum of the accelerated ions is of fundamental interest.

Extensive theoretical and computational work on the acceleration mechanisms has been pursued. Trajectories of ions have been studied in the crossed electric and magnetic fields generated in a collapsing z-pinch [10, 11]. The collapse of the plasma sheath, such as in a compressional Z-pinch, has also been taken into account [12]. In a different approach, reflections on the conical collapsing plasma sheath are held responsible for the acceleration [13]. Trubnikov and Vikhrev have debated on the origin of different fields produced by plasma instabilities [14, 15]. Recently, the acceleration of both electrons and ions in a plasma focus through magnetohydrodynamic (MHD) instabilities has been studied using a 3D relativistic and fully electromagnetic particle in cell code [16]. It is likely that more than one acceleration mechanism is in effect during the discharge.

In this work we shall revisit a model based on the development of the $m = 0$ instability proposed by Haines [17], in the framework of Hall-magnetohydrodynamics (HMHD), where finite Larmor radius effects are taken into account. The main feature is the existence of an asymmetry along the z-axis, which causes ions near the symmetry axis to be preferentially accelerated opposite the anode. This arises from the average axial drift of off-axis ions due to the radial electric field $Zn_i eE_r = \partial p_i/\partial r$. The axial flow has to be balanced by an equal and opposite flow of ions on-axis that have singular orbits. In order to account for this effect it is necessary to include the Hall term in Ohm's law as well as the electron pressure term, since these are the ones that break the symmetry. However, the assumption of no longitudinal plasma flow made in [17] is inconsistent with momentum equations, as we will show. If the axial velocity is zero, then there is no possibility of neck formation. In this paper we consider a model based on Haines' idea, that allows for a finite axial velocity to develop as the instability grows. Our model solves the HMHD equations for a cylindrical plasma column, initially in equilibrium, after a pinching perturbation is applied.

The paper is organized as follows. In section 2 we present the model used to study the development of the sausage instability and explain why it is necessary to include the axial plasma velocity in the computations. In section 3 we present the behavior of the plasma column and the resulting electric fields for several cases of interest. Section 4 is devoted to the computation of the ion orbits in the electromagnetic fields obtained in section 3 finding the accelerations they can achieve. Finally, in section 5 we give the conclusions of our work.

2. Mathematical model for the $m = 0$ instability

The first issue we have to address is to determine how the sausage instability develops in the plasma column, in order to obtain the electromagnetic fields that will act upon the ions. We model the $m = 0$ instability using the MHD equations including the Hall term in Ohm's law, as this is the one that accounts for the asymmetry along the axial direction resulting

from the singular-orbit ions; the Hall and the electron pressure gradient terms have mixed parities. The HMHD model has also been considered recently to study z-pinch equilibria and stability (see, e.g. [18] and references therein). However, while most works have done analytical estimates of stability, a numerical analysis of the evolution of the plasma has not been performed, to our knowledge. The model we study here is a reduced one that neglects thermal conductivity and, unlike [18], we do not study the stability conditions, but start from a potentially unstable equilibrium state. Our aim is mainly to estimate the electric fields produced during the development of the instability including the Hall term, and we do not expect them to be much influenced by the inclusion of heat transfer, due to the fast collapse time. For the analysis, we use a cylindrical plasma column having complete axisymmetry (i.e. $\partial/\partial\theta = 0$), carrying a uniform constant axial current I, with radius a and an azimuthal magnetic field $\boldsymbol{B} = B_\theta(r)\hat{\theta}$, given by $B_\theta = 2Ir/ca(z)^2$ for $r < a$ and $B_\theta = 2I/cr$ for $r > a$. The corresponding equations for the density, ρ, radial velocity, v_r and axial velocity, v_z, are

$$\frac{\partial \rho}{\partial t} = -\frac{1}{r}\frac{\partial}{\partial r}(r\rho v_r) - \frac{\partial}{\partial z}(\rho v_z), \tag{1}$$

$$\rho\left(\frac{\partial v_r}{\partial t} + v_r\frac{\partial v_r}{\partial r} + v_z\frac{\partial v_r}{\partial z}\right) = -\frac{\partial p}{\partial r} - \frac{J_z B_\theta}{c}, \tag{2}$$

$$\rho\left(\frac{\partial v_z}{\partial t} + v_r\frac{\partial v_z}{\partial r} + v_z\frac{\partial v_z}{\partial z}\right) = -\frac{\partial p}{\partial z} + \frac{J_r B_\theta}{c}, \tag{3}$$

where $J_z = (I/\pi a^2)$ and $J_r = (Ir/\pi a^3)\partial a/\partial z$, follow from Ampere's law, $J_r = (c/4\pi)\partial B_\theta/\partial z$ and B_θ given above. As the plasma evolves, the associated electric fields are obtained from Ohm's law as

$$E_r = \frac{v_z B_\theta}{c} + \eta J_r - \frac{J_z B_\theta}{nec} - \frac{1}{ne}\frac{\partial p_e}{\partial r}, \tag{4}$$

$$E_z = -\frac{v_r B_\theta}{c} + \eta J_z + \frac{J_r B_\theta}{nec} - \frac{1}{ne}\frac{\partial p_e}{\partial z}, \tag{5}$$

where η is the resistivity. We do not use an energy equation and the system is closed using a polytropic equation for the pressure: $p = k\rho^\gamma$ with γ a free parameter. Depending on the value of γ we can analyze different thermal situations. The most appropriate in this case is to use $\gamma = 2$ which represents an adiabatic process in two dimensions, due to the axisymmetry and the fast timescales involved. However, by using $\gamma = 1$ we could study isothermal processes (but they would not be expected to occur, which is actually supported by our numerical results).

The reduced model we use is obtained by assuming that the axial electric current is fixed and thus the magnetic field has only an azimuthal component which evolves according to the variation of the plasma radius $a(z, t)$, i.e. $B_\theta(r, z, t) = 2Ir/ca(z, t)^2$ with $I =$ constant. The variables in the model are the mass density, $\rho(r, z, t)$, the radial and axial velocities, $v_r(r, x, t)$, $v_z(r, z, t)$, and the column radius $a(z, t)$. The equation for $a(z, t)$ follows from Faraday's law together with Ohm's law. The four governing equations in dimensionless form are

$$\frac{\partial \rho}{\partial t} = -\frac{1}{r}\frac{\partial}{\partial r}(r\rho v_r) - \frac{\partial}{\partial z}(\rho v_z), \tag{6}$$

$$\frac{\partial v_r}{\partial t} = -v_r\frac{\partial v_r}{\partial r} - v_z\frac{\partial v_r}{\partial z} - \frac{I^2}{\rho}\frac{r}{a^4} - \gamma\rho^{\gamma-2}\frac{p}{\rho_c^\gamma}\frac{\partial \rho}{\partial r}, \tag{7}$$

$$\frac{\partial v_z}{\partial t} = -v_r\frac{\partial v_z}{\partial r} - v_z\frac{\partial v_z}{\partial z} + \frac{I^2}{\rho}\frac{r^2}{a^5}\frac{\partial a}{\partial z} - \gamma\rho^{\gamma-2}\frac{p}{\rho_c^\gamma}\frac{\partial \rho}{\partial z}, \tag{8}$$

$$\frac{\partial a}{\partial t} = \frac{a^3}{2}\frac{\partial}{\partial z}\left(\frac{v_z}{a^2}\right) + \frac{a}{2r}\frac{\partial}{\partial r}(r v_r) + A_2\eta\frac{\partial^2 a}{\partial z^2} - A_2\frac{3\eta}{a}\left(\frac{\partial a}{\partial z}\right)^2$$
$$- A_1 I a^3 \frac{\partial}{\partial z}\frac{1}{\rho a^4} - -A_1\frac{I}{r a^2}\frac{\partial a}{\partial z}\frac{\partial}{\partial r}\left(\frac{r^2}{\rho}\right), \tag{9}$$

with the coefficients,

$$A_1 = \frac{m I a^3 t_0}{2\pi e \rho_0 L^3}, \qquad A_2 = \frac{\eta c^2 t_0}{4\pi L^2}.$$

The variables are normalized according to the following: $\rho \to \rho/\rho_0$, $v \to v t_0/L$, $a \to a/L$, $r \to r/L$, $z \to z/L$, $t \to t/t_0$, $I \to I/I_0$, $p \to p/p_0$ and $\eta \to \eta/\eta_0$. Here, L and t_0 are characteristic scales of length and time, and the other normalization constants are fixed according to typical values in a z-pinch, as $\rho_0 = m_i n = (3.34 \times 10^{-24}\,\mathrm{g})(10^{18}\,\mathrm{cm}^{-3}) = 3.34 \times 10^{-6}\,\mathrm{g\,cm}^{-3}$, $I_0 = (\pi\rho_0/2)^{1/2}(cL^2/t_0)$, $p_0 = \rho_0 L^2/t_0^2$ and $\eta_0 = \eta(T = 20\,\mathrm{eV}) = 10^{-15}\,\mathrm{s} = 9 \times 10^{-4}\Omega\,\mathrm{cm}$. The time scale is a measure of the Alfvén time associated with L, $t_0 \sim t_\mathrm{A} = L/v_\mathrm{A} = L\sqrt{4\pi\rho}/B \sim \sqrt{\pi\rho_0}cL^2/I_0$.

In obtaining equation (9) we assumed that the electron pressure also follows a polytropic equation of the type used for the total pressure ($p_e = k_e\rho^{\gamma_e}$), in order to keep the same number of variables. With this assumption the p_e terms in equation (9) cancel out and do not contribute to it. These terms only appear in the expression of the induced electric field but do not affect the evolution of the plasma.

The reason why the assumption of $v_z = 0$ is inappropriate can be understood in two ways. First, if one considers the same dependences used by Haines [17], where the radial velocity has the form $v_r = (r/a)(\mathrm{d}a/\mathrm{d}t)$ and the mass density is expressed in terms of the line number density N through $\rho = N m_i/\pi a^2$, an integration of the momentum equations (2) and (3), when taking $v_z = 0$, leads to the following two equations for pressure:

$$p = -\left[\frac{N m_i}{2\pi a^3}\frac{\partial^2 a}{\partial t^2} + \frac{I^2}{\pi c^2 a^4}\right] r^2 + f(z), \tag{10}$$

$$p = -\frac{I^2 r^2}{2\pi c^2 a^4} + g(r). \tag{11}$$

These equations can only be simultaneously satisfied if the two integration functions, $f(z)$, $g(r)$, are actually constants, implying that the pressure has a parabolic profile, if the boundary condition $p(r = a, z, t) = 0$ is to be satisfied,

$$p(r, z) = \frac{I^2}{2\pi c^2 a^2}\left(1 - \frac{r^2}{a^2}\right).$$

But then, the coefficient $I^2/(2\pi c^2 a^2)$ has to be constant in order to comply with equation (8), which implies $\mathrm{d}a/\mathrm{d}z = 0$. This means there is no possibility of neck formation.

Second, in the more general case when no assumptions are made about the form of the radial velocity, it is noticed that when $v_z = 0$, equation (3) gives $\partial p/\partial z = J_r B_\theta/c$. When we substitute the expressions of J_r and B_θ in terms of $a(z)$ and the polytropic equation for p we obtain the proportionality,

$$\frac{\mathrm{d}a}{\mathrm{d}z} \propto \frac{\partial \rho}{\partial z}.$$

However, the neck formation should produce the opposite effect since as one moves along z to the narrow region ($\mathrm{d}a/\mathrm{d}z < 0$) the density should increase ($\partial\rho/\partial z > 0$). Thus a finite value of v_z is necessary.

The magnitude of the coefficients A_1 and A_2 determines the relative importance of the Hall and resistive terms, respectively, in the evolution of the column radius. Nevertheless, the contribution of these terms, as well as the p_e-term in the electric fields, are of different order. They can be written in terms of the normalized variables as

$$E_r = A_3 \frac{v_z I r}{a^2} + A_4 \eta \frac{I r}{a^3} \frac{\partial a}{\partial z} - A_5 \frac{I^2 r}{\rho a^4} - A_5 \frac{\gamma_e}{\rho_c^{\gamma_e}} \frac{f_e p}{\rho^{2-\gamma_e}} \frac{\partial \rho}{\partial r}, \tag{12}$$

$$E_z = -\frac{v_r I r}{a^2} + A_4 \eta \frac{I}{a^2} + A_5 \frac{I^2 r^2}{\rho a^5} \frac{\partial a}{\partial z} - A_5 \frac{\gamma_e}{\rho_c^{\gamma_e}} \frac{f_e p}{\rho^{2-\gamma_e}} \frac{\partial \rho}{\partial z}, \tag{13}$$

where

$$A_3 = \frac{L^2 \sqrt{2\pi \rho_o}}{c t_0^2}, \qquad A_4 = \frac{c \eta_0}{t_0} \sqrt{\frac{\rho_0}{2\pi}}, \qquad A_5 = \frac{m_i L}{e t_0^2}$$

are the coefficients that weigh the relative importance of the motional E-field term, the resistive term and the Hall and p_e terms (both are of the same size). The electron pressure is taken as a fixed fraction of the total pressure, $f_e = p_e/p$ and it is set to $f_e = 0.5$ for all cases studied.

Equations (6)–(9) are solved in a domain that includes the plasma and the vacuum region, covering the range $r = (0, L)$ and $z = (-L, L)$. The electric fields are computed only within the plasma region since the ions cannot reach the vacuum region because of the strong electrostatic forces. Only when the particles are accelerated to very high energies can they leave the plasma.

The numerical scheme followed is based on a leapfrog trapezoidal algorithm, with a predictor–corrector evolution. The boundary conditions in the z direction are periodic for all variables except v_z, for which we set $\partial v_z/\partial z = 0$, which is used to avoid axial plasma acceleration at the domain boundary assuring a regular behavior for v_z. In the radial direction we imposed the condition $v_r(r = 0) = 0$, while for the other variables the radial derivative was set equal to zero at $r = 0$. For the vacuum region we assumed free-flow boundary conditions, that is, $\partial \xi/\partial r$ is continuous at the domain boundary. The perturbation is applied as a small sinusoidal radial velocity: $v_r(r, z, t = 0) = V_{r0} r \cos^2(kz)$. The free parameters that we can vary are the total current I and the pressure P. In the calculations presented here we used $V_{r0} = 0.5$ (normalized to L/t_0) and $k = \pi/2L$. The initial density profile is set to a parabolic shape, $\rho(r, z) = \rho_0(1 - (r/a)^2)^{1/\gamma}$, which results from the equilibrium condition given by equation (7) when $v = 0$. Of course, this initial equilibrium is destroyed when the perturbation is applied and we follow the evolution of the plasma column. We also tested a flat profile ($\rho(r, z) = \rho_0$) which would correspond to a skin current confined to the plasma boundary.

3. Plasma dynamics results

Most of our computations were done for parameters of a typical z-pinch plasma and we just varied some of the values for the most relevant variables. One of these parameters is the plasma radius a, as this is the one that determines the relative importance of the Hall term, for it will have a sizable contribution when a is of the order of the ion Larmor radius, $a \sim r_L$. The first computation we show is for $a = 1$ cm and we take $L = 1$ cm, thus having the normalized radius $\hat{a} = 1$. The other parameters are $t_0 = 3 \times 10^{-8}$ s, $I_0 = 2.29 \times 10^{15}$ esu $= 760$ kA, $p_0 = 3.7 \times 10^9$ dyn cm^{-2}, and we set the total current equal to 190 kA, i.e. $I = 0.25$, while the central pressure is set by $p = 0.03$, giving an absolute value of 1.1×10^8 dyn cm$^{-2} = 82.5$ kTorr. The corresponding temperature, obtained

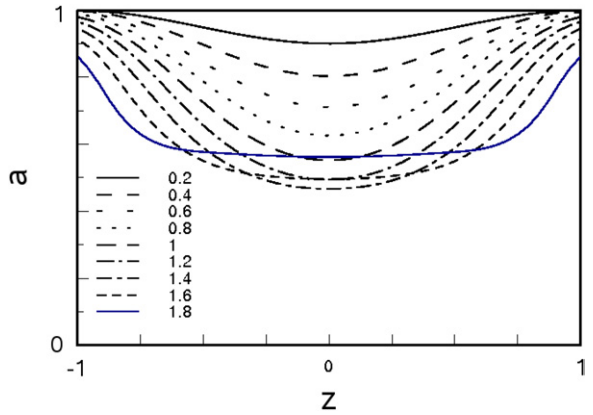

Figure 1. Evolution of the plasma column radius for initial $a = 1\,\mathrm{cm} > r_L$. Times indicated at the different stages are normalized to $t_0 = 30\,\mathrm{ns}$. Current is $I = 190\,\mathrm{kA}$ and pressure $p = 82.5\,\mathrm{kTorr}$.

(This figure is in colour only in the electronic version)

from the equation of state, turns out to be about 70 eV. For the normalized electrical resistivity we used $\eta = 1/2$, but this term is quite unimportant. The values of the polytropic index were varied and the best compression was obtained for $\gamma = 2$ corresponding to a 2D adiabatic evolution, as expected. For these parameters, the Larmor radius is of the order of 1 mm, so we do not expect the Hall terms to be important in the development of the instability. The typical case has a parabolic density profile and the evolution of $a(z, t)$ is shown in figure 1. It is seen that the column develops a neck which decreases its width until it reaches a minimum value in a time of the order of the Alfvén time (about 30 ns). After the maximum narrowing, the column rebounds making the neck almost disappear. For this case the instability develops with a complete symmetry about $z = 0$, so both sides of the neck are equal. This is what would be expected when the Hall terms are negligible. The dependence of the plasma density is shown in figure 2. We can see that the maximum compression is 5 times the initial central density.

On the other hand, the velocity field and the resulting electric fields, for the maximum compression, can be seen in figures 3 and 4. The magnitudes of both fields are largest near the boundary due to the large pressure and velocity gradients there. The velocity has an important z-component both at the edge and close to the central axis ($r = 0$). In particular, it is of interest to notice the orientation of the electric field vectors. In contrast to what happens in the evolution of the plasma radius, the Hall term does have a noticeable effect. The direction of E_z changes at the negative side of the neck due to the contribution of the Hall and p_e terms, since the inductive term $(\boldsymbol{v} \times \boldsymbol{B})$ in equation (13) is positive everywhere (recall $v_r < 0$). Meanwhile, the sign of E_r varies in the same way as the sign of v_z, indicating that the inductive term in equation (12) is dominant and that the inclusion of v_z in our model is really important. The Hall and pressure terms have some contribution to E_r but of minor importance. It is then clear that there is an asymmetry in z introduced by the Hall term.

In the simulations we tried cases where the initial radius extended up to the last cell of the computational radial range, which means there is no external vacuum region; but we also considered cases with $a(t = 0) < L$ which leaves some space with zero density beyond the outer edge. Apart from the possible influence of certain boundary conditions imposed at $r = 1$, there was no difference between the two cases.

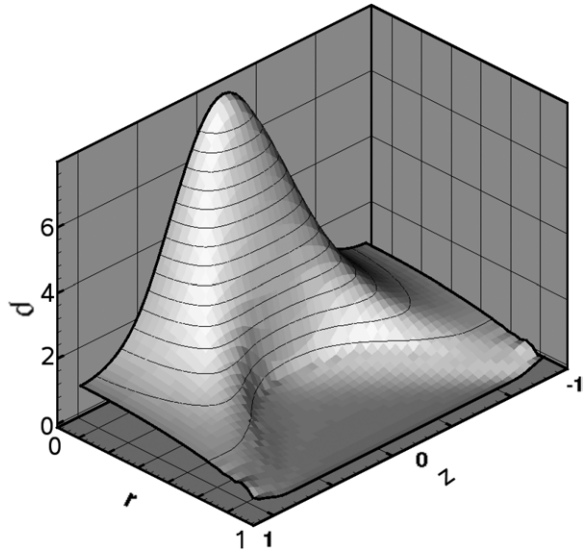

Figure 2. Density profile $\rho(r, z)$ for a high initial pressure near the end of the compression. It increases mainly close to the axis at the neck position.

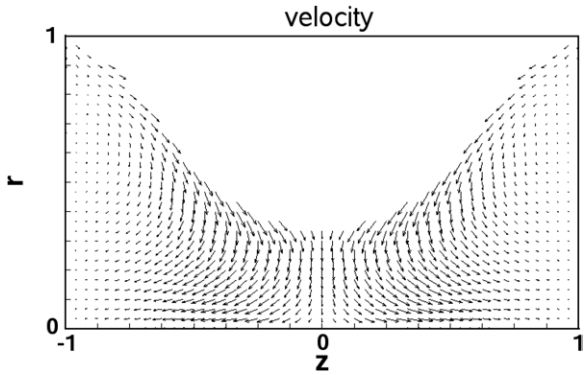

Figure 3. Velocity vectors at the time of maximum compression for the same parameters of figure 1. An axial velocity has developed and it has an odd parity in z, as expected.

We also performed computations for an initially flat density profile, roughly simulating a skin current distribution. The results for a and ρ are similar to the parabolic profile but the maximum ρ and the minimum a are larger due to the fact that there is more matter to sweep by the compressing neck. But for the same reason, the compression slows down more intensely leading to a shorter time for maximum narrowing. In the expansion stage, after the minimum radius is reached, there is a bulging at the neck due to the larger pressure that has built up. The complete evolution is shown in figure 5. An important difference is that the E-fields from equations (12) and (13) nearly vanish since $I \approx 0$ inside the plasma. Thus, this case would not be useful to study ion acceleration in HMDH.

The next step was to reduce the column radius relative to r_L. In order to keep $r_L \sim 1$ mm the magnitude of the B-field has to be kept the same, which requires the current to scale directly with L (since $B \sim I/L$). Thus, by fixing $L = 0.1$ cm we have to set $I = 19$ kA.

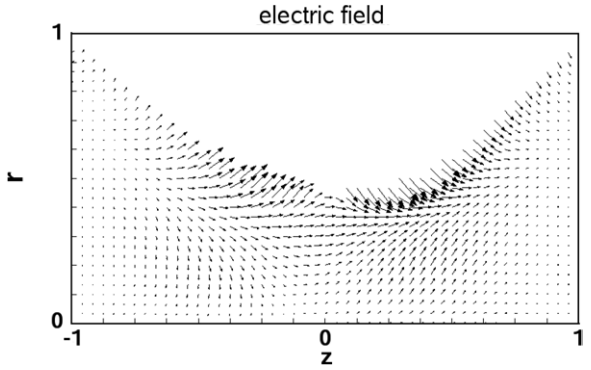

Figure 4. Elecric field vectors at the end of the instability for the same case of figure 1. Note that the point of reversal of E_z is located to the left of the neck, showing the asymmetry in z.

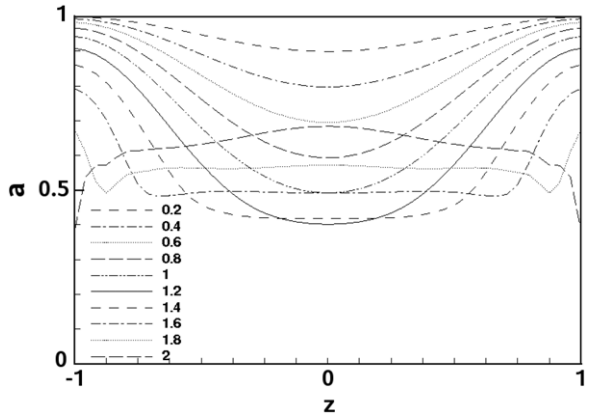

Figure 5. Evolution of the plasma column radius for a flat density profile, an initial radius $a = 1$ cm and total current $I = 190$ kA. Times indicated in the legends are normalized to $t_0 = 30$ ns. At the final stage it resembles a narrow column with no noticeable neck.

Also, to maintain the initial equilibrium condition the pressure has to stay at the same value of $p = 82.5$ kTorr. In this case the evolution is faster than the one for $L = 1$ cm, since the characteristic time also scales as $\sim L$ and thus is smaller by an order of magnitude: $t_0 = 3$ ns. For this case we used an initial radius $a(t = 0) = 0.9$ leaving an initial outer vacuum region. The results show there is a more important effect of the Hall and resistive terms on the evolution of $a(t)$, as expected, but still they are not dominant (the coefficients in equation (9) are $A_1 = 0.23$, $A_2 = 0.021$). Therefore, in figure 6 we chose to show the evolution of the plasma radius for the extreme case of $a(t = 0) = 0.01$ cm where the Hall terms dominate and thus their effect is seen more clearly (now $A_1 = 2.3$, $A_2 = 0.21$). The first thing to notice is the left-right asymmetry in the compression, coupled to a displacement to the right of the minimum and maximum positions. This is more evident near the later stages of the evolution, when the neck is expanding. The reason for this can be traced back to the term $\partial\rho/\partial z$ in equation (9), which means it is related to the appearance of the high-density spot (hot spot) at the center. For this case we can also examine the electric vector field, shown in figure 7 for the time of maximum compression ($t = 1.4$), noticing a dramatic change with respect to the previous case. Now the effect of the Hall term is more important, which makes E_r to be negative near the plasma

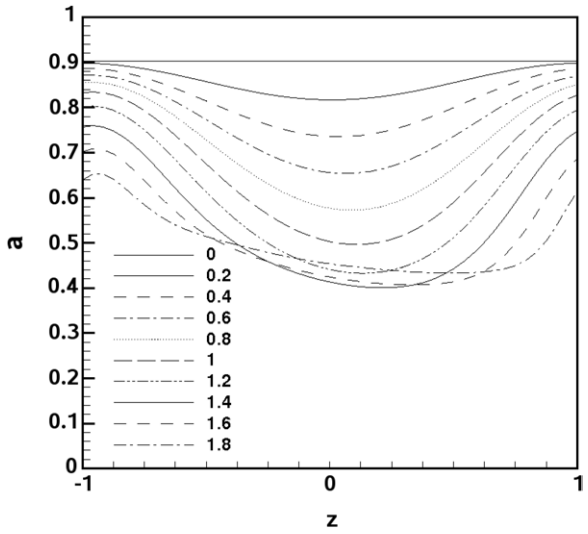

Figure 6. Evolution of the plasma column radius for initial $a = 0.01\,\mathrm{cm} < r_\mathrm{L}$, $I = 1.9\,\mathrm{kA}$ and $p = 82.5\,\mathrm{kTorr}$. Times of the different stages indicated are normalized to $t_0 = 0.3\,\mathrm{ns}$.

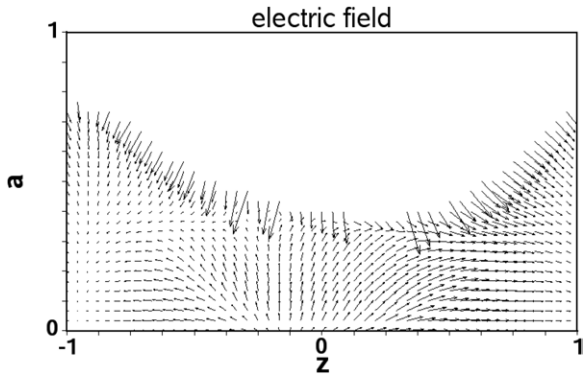

Figure 7. Electric field vectors for initial $a = 0.01\,\mathrm{cm}$ at the time of minimum neck radius $t = 1.4t_0 = 0.42\,\mathrm{ns}$, for the same parameters of figure 6. The fact that $E_z(-z) = -E_z(z)$ over most part of the volume reveals a predominance of the Hall and p_e terms.

edge, while the p_e term is dominant near the central high-density region ($r \approx z \approx 0$). If the non-inductive terms were already of relevance when $a = 1\,\mathrm{cm}$, in determining the E-field, now they have become dominant over most part of the plasma volume. But the asymmetry in the position of the reversal of E_z still prevails, which shows that the inductive terms are not completely negligible.

Another test we have made is to modify the polytropic index in order to simulate different thermal conditions. So far, the value of $\gamma = 2$ used would correspond to a 2D adiabatic process, which appears to be the appropriate one given the symmetry in the angle θ. When we use $\gamma = 5/3$ (3D adiabatic), the evolution is somewhat slower and it takes longer to reach maximum compression, but the central density is higher. On the other hand, for $\gamma = 3$ (1D adiabatic) there is less compression, obtaining a relatively wide neck and low central density. However, the overall results do not change much among these three cases. It is worth mentioning that

when we set $\gamma = 1$, corresponding to an isothermal process, there is no regular evolution and the column collapses. This would indicate the impossibility of isothermal evolution due to the fast time scale involved, i.e. no heat transport takes place, as mentioned at the beginning of section 2.

Before turning to the problem of ion acceleration it is necessary to determine the collisional regime of the plasma. For the parameters used in this section the collisional mean free path λ_c is smaller than the system size L, which would require to include collisions in computing ion trajectories. However, collisions can be neglected for higher pressure plasmas. When $T = 1$ keV and $n = 10^{18}$ cm^3, which in fact are quite common values in z-pinches and plasma foci, $\lambda_c = 2$ cm $> L$. We have made computations for this high pressure, obtaining very similar results to those shown here, but with a smaller compression rate. We chose to show the results for lower pressures to make more evident the compression effects, but we will assume in the next section that we are in the high pressure regime in order to apply the collisionless orbit theory.

4. Ion orbits

Once the $m = 0$ instability develops, the resulting electromagnetic fields act upon the charged particles, and thus ions can eventually be accelerated. In order to obtain the ion orbits and determine the acceleration rate we solve the ion equations of motion for a single particle, which in cylindrical coordinates are

$$\frac{\partial v_r}{\partial t} = \frac{Ze}{m_i}(E_r - v_z B_\theta) + \frac{h}{r^3}, \tag{14}$$

$$\frac{\partial v_z}{\partial t} = \frac{Ze}{m_i}(E_z - v_r B_\theta), \tag{15}$$

where $h = r^2\dot{\theta}$ is the specific angular momentum, a constant of motion. As mentioned above, near the region of neck formation there are two kinds of particle orbits drifting in opposite directions: off-the-axis ions drifting from cathode to anode and singular-orbit ions located within a Larmor radius of the axis. The latter are less numerous but have higher speeds. We have numerically solved equations (14) and (15) for the electric and magnetic fields obtained from the instability development, confirming the presence of the two types of orbits. The E-fields used are those reported in section 3 for both $L = 1$ cm and $L = 0.1$ cm. The example shown in figures 6 and 7 for $L = 0.01$ cm is not used here since the Larmor radius is larger than a and thus no particles can move within.

First we consider the fields due to the column with $a = 1$ cm given in figure 4. In figure 8 we show, with a continuous line, the orbit of an off-axis ion with an energy $W = 80$ eV. There is a grad-B drift to the left but there is practically no energy gain as can be evidenced by the velocity path shown in the same figure by the dashed line. The distance from the coordinates origin is a measure of the ion speed, and hence the energy. Now, for ions located close to the axis (less than one Larmor radius, which in the vicinity of the axis, where $B = 3$ T, is of the order of 0.03 cm) the orbit is snake-like moving to the right, regardless of which side of the neck it starts from, as can be seen in figure 9. The ion energy is 80 eV and it starts at the left side of the neck moving right until it leaves the instability region. The energy gained by the ion is appreciated in the velocity trajectory plot depicted by the dashed line: the distance from the origin keeps increasing. In a couple of orbits the ion energy goes up by a factor of 23 to 1.8 keV. It is also apparent that the velocity increases predominantly to the z-direction and thus the pitch angle gets reduced on each cycle. This is characteristic of an axial acceleration produced by the axial electric field.

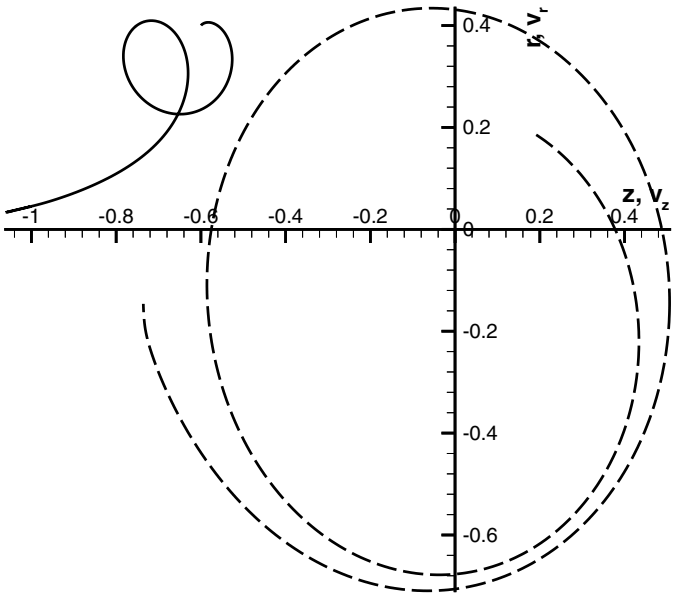

Figure 8. Off-axis ion orbit (solid line) with energy 80 eV starting at $(r_0, z_0) = (0.4, -0.6)$ cm and velocity vector having a pitch angle of 45° with the cylinder axis, drifting to the left. Velocity space trajectory (dashed line) is also shown.

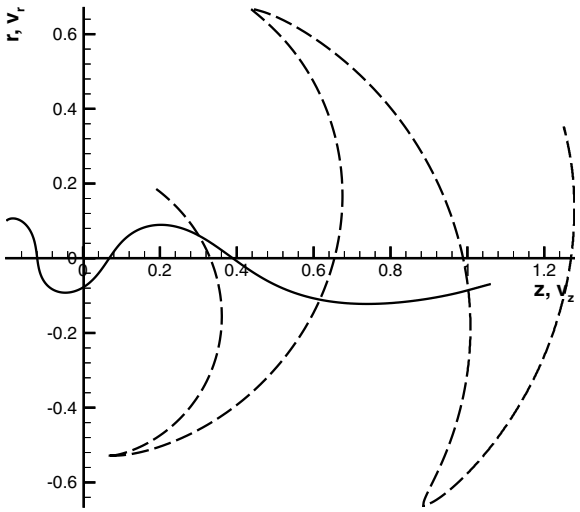

Figure 9. Singular orbit (solid) of on-axis ion having an initial pitch angle of 45°, in a thick column, drifting to the right. Velocity path (dashed) shows the energy gain.

There is a third type of ion orbit which we found to be the most common of all. It is possible for an ion to transit from an off-axis orbit to a singular orbit when the starting point is close to the region where the E-field has a large axial component. This mixed orbit is shown in figure 10 which starts being non-singular, but drifts toward the column axis as a result of the $E \times B$ drift; it then crosses the axis and the orbit becomes singular thus gaining more energy. When the trajectory starts at or to the right of the neck the energy gain is modest,

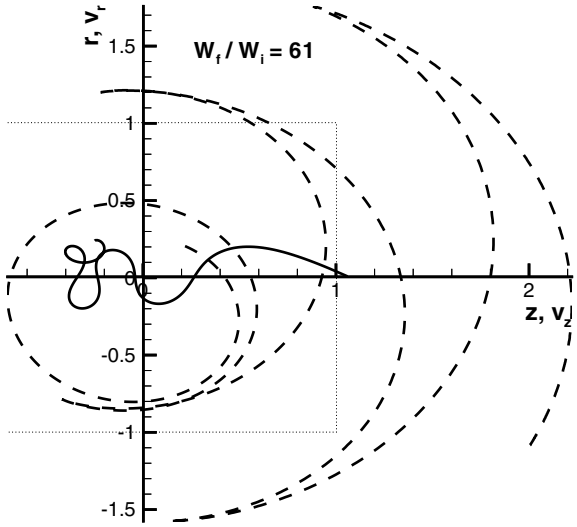

Figure 10. Mixed orbit for ion close to the plasma border transiting to snake-like path having a high energy gain. The initial energy is 100 eV and the pitch angle is 45°. Notice the large final velocity, seen at the end of the dashed line. The dotted box indicates the plasma column volume.

but for initial positions with $z < 0$, as in the case shown, the ion has large energy gains since they get accelerated through most part of the plasma column. Here the initial energy is $W = 0.1$ keV and there is an energy gain of 62, ending up with an energy of 6.2 keV, as it leaves the simulation region (shown by a dotted box). The velocity space evolution (dashed curve) shows again the change in orbit type and how energy is increased, just as the symmetry axis is reached.

Now we turn to the case of a thin column with $a = 0.09\,\text{cm} \sim r_\text{L}$. The electric fields have a configuration very similar to those shown in figure 7. Nevertheless, the distinction between regular and singular orbits does not apply here since all ions have to stay within a Larmor radius if they are to stay inside the plasma. The influence of the E-fields is more important now than in the thicker column. Clearly the guiding-center approximation is not applicable here and the orbits cannot be described in a simple way. For the different initial positions and pitch angles the particles cannot gain much energy before leaving the region. It is to be noticed that the length of the axial region is quite small ($L \sim 2$ mm) and there is not much time for the ions to gain energy. Many of the orbits soon leave the field region either radially or axially with no energy gain or with energy loss. Roughly, ions that start to the right of the point of E_z reversal leave at the right end, and those starting to the left leave at the left end, due to the large influence of E_z, but the latter have no energy gain. The fact that $E_r > 0$ prevents many off-axis ions from reaching the axis and become singular. In figure 11 there is a representation of two orbits of 100 eV ions (solid and dash–doted lines), together with their respective velocity paths (dashed and dotted lines). The orbits are of the snake type, like the singular orbits of the previous case, but they are due to the large E_z-field. Both have modest energy gains with $W_f/W_i = 6.2$ and 7.8; the former crosses the axis and travels a longer distance but the acceleration is less than the latter, since the one that does not cross the axis has a more efficient effect of the electric field. This exemplifies the complexity and non-uniformity of ion orbit characteristics. If the axial length of the perturbation is scaled up one order of magnitude to a few centimeters, the acceleration of snake-like orbits would take

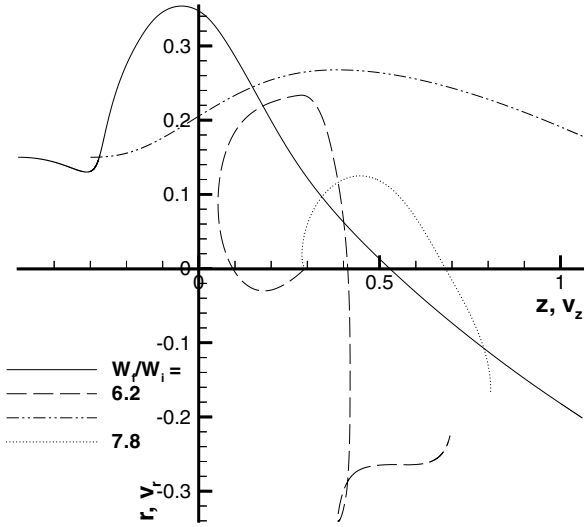

Figure 11. Ion orbits in a thin column for two initial positions (solid and dash–dotted lines) for the same energy 100 eV and initial velocity parallel to the axis. Velocity space trajectory for each particle (dashed and dotted lines).

place for a longer time and the final energies would be an order of magnitude larger: 62 and 78 fold gains for the cases of figure 11. Therefore, it is comparable to the values obtained for the 1 cm plasma column.

5. Conclusions

The $m = 0$ instability of a cylindrical plasma column has been studied using a model based on HMHD. The parameters that have been varied are the total plasma current (which stays constant throughout the time evolution and in the plasma cross section), the central pressure and density, initial plasma radius, pressure profile and polytropic index. Under different situations the behavior of the column was analyzed, obtaining the characteristic features of the instability and the resulting electric fields. Due to the presence of the Hall and p_e terms, the E-fields present a left–right asymmetry in the z-direction around the neck, having always, near the axis, a reversal point of the axial direction at the anode side of the plasma neck. For a thick initial column ($L = 1\,\text{cm} > r_\text{L}$) the Hall terms are not important in determining the dynamics of the plasma but they do affect the E-field. When the column radius is of the same size of the Larmor radius ($L = 1\,\text{mm} \sim r_\text{L}$) the evolution of the plasma column is very much affected by the Hall and p_e terms, the neck being shifted toward the cathode and losing the left-right symmetry; the E-field is totally dominated by these terms having a distribution very different from the one for a thick column. Both the plasma velocity and the E-field have quite large magnitudes at the edge of the contracting plasma due to the high-density gradient produced there. The density itself increases strongly at the center of the neck but for some, large amplitudes of the perturbation velocity, it can also have a shock-like maximum at the edge. Central density and pressure can have an 8-fold increase. The inclusion of an axial velocity in our model turns out to be quite important, as this is responsible for producing the large E_r component of the field which has a large impact on the ion orbits. However, for the thin column, the dominance of

the Hall and p_e terms over the inductive term (containing v) renders the influence of the axial velocity negligible.

A point briefly mentioned was the extension of our simple model to a more realistic case with a non-constant current. The initial current profile in a plasma focus is concentrated to the edge and the penetration time is large relative to the instability growth time. Therefore, our results would only apply to the subsequent instabilities, excited when the current has already homogenized. For early times, a rough idea of what to expect for a skin current may result by using a flat pressure profile, which produces no electric fields (except for the induction E-field), and therefore no ion acceleration of the type we were considering. The inclusion of variable current should be studied in a future work.

Regarding the motion of the ions in the electric fields due to the instability, we only consider the collisionless motion of the particles, bearing in mind that it is applicable only for high pressure discharges. We found different results for the thin and thick columns. In the thick plasma column the Larmor radius is smaller than a and therefore there can be two different types of orbits. Off-axis ions drift toward the anode but do not get accelerated much. On-axis ions have singular orbits embracing the axis moving toward the cathode and these can have large energy gains. But a large fraction of off-axis ions can drift toward the axis by the effect of the E_z field and once there their orbits become singular and have the largest energy increments: over 60 fold (especially those to the left of the neck). Taken together, an important fraction of ions can be accelerated to high energies. An effect the finite v_z has on the orbits, through its influence on E_r, is that some off-axis ions do not get much acceleration. On the other hand, for a thin column of the order of r_{L}, the orbits cannot be separated in the two previous types since all are close to the axis. The E-fields affect more strongly the shape of the orbits and the large E_z component close to the axis causes important acceleration in the direction of the cathode. The ions starting close to the anode do not have acceleration. When scaled up to column lengths of the same size, thin and thick plasmas produce similar energy gain values.

Our results thus confirm the prediction mentioned in section 1 made by Haines [17], in the sense that on-axis ions moving toward the cathode should appear in order to offset the current of off-axis drifting ions. Additionally, we also obtain the same conclusion for thin columns where there is no separation between off- and on-axis ions: still the current of high energy particles is toward the cathode. They are presumably responsible for the beam–target fusion reactions.

Acknowledgments

This work was partially supported by DGAPA-UNAM project IN119408.

References

[1] Thoneman P C *et al* 1958 *Nature* **181** 217
[2] Hagerman D C and Mather J W 1958 *Nature* **181** 226
[3] Burkhardt A and Loveberg R H 1958 *Nature* **181** 228
[4] Rose B, Taylor A E and Wood E 1958 *Nature* **181** 1630
[5] Mather J W 1971 *Methods in Experimental Physics* (New York: Academic) vol 9B p 187
[6] Filippov N V 1983 *Sov. J. Plasma Phys.* **9** 14
[7] Bernard A *et al* 1998 *Moscow Phys. Soc.* **8** 93
[8] Castillo F *et al* 2000 *J. Phys. D: Appl. Phys.* **33** 141
[9] Castillo F *et al* 2003 *Plasma Phys. Control. Fusion* **45** 289
[10] Bernstein M J 1970 *Phys. Fluids* **13** 2858

[11] Garry S P and Hohl F 1973 *Phys. Fluids* **16** 997
[12] Kondoh Y and Hirano K 1978 *Phys. Fluids* **21** 1617
[13] Deutsch R and Kies W 1988 *Plasma Phys. Control. Fusion* **30** 263
[14] Trubnikov B A 1986 *Fiz. Plazmy* **12** 468
[15] Vikhrev V V, Ivanov V V and Rozanova G A 1989 *Fiz. Plazmy* **15** 77
[16] Haruki T, Yousefi H R, Masugata K, Sakai J-I, Mizuguchi Y, Makino N and Ito H 2006 *Phys. Plasmas* **13** 082106
[17] Haines M G 1983 *Nucl. Instrum. Methods* **207** 179
[18] Shtemler Y M and Mond M 2006 *J. Plasma Phys.* **72** 699